Current density measurements in Tokamak devices

1992 Plasma Phys. Control. Fusion 34 1669

(http://iopscience.iop.org/0741-3335/34/12/001)

Plasma Physics and Controlled Fusion, Vol. 34, No. 12, pp. 1669 to 1698, 1992
Printed in Great Britain.

0741-3335/92 $5.00+ .00

REVIEW ARTICLE

CURRENT DENSITY MEASUREMENTS IN TOKAMAK DEVICES

H. SOLTWISCH
Institut für Plasmaphysik, Forschungszentrum Jülich GmbH, Association EURATOM–KFA, Postfach 1913, D-5170 Jülich, Germany

(*Received* 3 *February* 1992; *and in revised form* 12 *May* 1992)

Abstract—Tokamak plasmas are, at present, the most studied objects in controlled thermonuclear fusion research. The basic concept of these devices relies on externally induced currents which serve the twofold purpose of heating the plasma and creating an appropriate magnetic field structure for confinement. Hence, a detailed knowledge of the current density distributions and the dependencies on the operational conditions are important for both the theoretical understanding and the practical improvement of Tokamaks. In this article, the experimental techniques for measuring the current density profile or the associated magnetic fields within the plasma are reviewed. After a brief description of the equilibrium magnetic field configuration in toroidal geometry and a short account of indirect and passive diagnostic methods, an assessment is made of the currently available techniques with respect to the state of development and the obtained results. Since none of the approaches has yet attained the standard of a routine diagnostic, only few systematic studies have been performed so far, and many observations stem from tests of the conceptual and practical feasibility of various methods. The findings are summarized in the final chapter.

1. INTRODUCTION

PLASMAS CONTAINED in a Tokamak configuration are susceptible to a large number of instabilities. Microscopic disturbances like fine-grained turbulences mainly cause an enhanced heat diffusion and deteriorate the confinement of energy. Macroscopic instabilities by spontaneous magneto-hydrodynamic deformations of the confining fields can lead to an abrupt termination of the plasma current and to a massive strain on the mechanical structure that has to take the suddenly released energy. In many cases, the appearance and growth rates of the instabilities are determined by details of the magnetic field pattern and hence by the distribution of the induced plasma current, although the theoretical understanding is far from being complete. Experimentally, the means to influence the current density profile are rather limited. Normally, one has to allow the Tokamak to itself establish the delicate balance between local power input and heat losses through radiation and transport across the magnetic surfaces, and to find a quasi-stationary equilibrium state with good confinement properties. The resulting performance is not always satisfactory, especially when undue amounts of impurity ions deform the electron temperature profile by localized radiation and affect the plasma conductivity. Thus, in order to guide the experimental efforts towards predictable, high-confinement regimes and to supply input information for concomitant theoretical investigations, a detailed knowledge of the current density distribution and its dependence on the operational conditions is of great importance.

Following the worldwide spread of Tokamak installations in the 1970s, many attempts have been made to develop techniques for measuring the current density profile or the associated magnetic fields within the plasma. However, none of the tried methods has yet attained the standard of a routine diagnostic—probably because the invoked physical principles or the required instrumentations turned out to be more complex than those for other plasma parameters (as, e.g. the electron temperature and density by Thomson scattering). A comprehensive survey of the early exploratory work was given by PEACOCK (1978) who stated in his introduction that "it would seem that the quest for a simple, reliable and accurate technique is still very actively being pursued". More than a dozen years later the situation is virtually unchanged, but by now the increased size and complexity of modern Tokamaks demand more elaborate equipment and restrict the latitude for improvised "proof in principle" experiments.

In this article, the present status of current density measurements in Tokamak devices is reviewed with respect to both the employed techniques and the obtained results. The latter refer primarily to the plasma core region where the axial current density and the related safety factor play a central role in understanding the sawtooth phenomenon. Experimental investigations of complete current density profiles and their implications for plasma confinement and stability have hardly been published so far. For this reason the material is organized into various methodic approaches rather than issues of Tokamak physics. We begin with a brief description of the equilibrium magnetic field structure in toroidal geometry in order to remind ourselves of the relevant quantities that we wish to measure. Next, we consider indirect and passive diagnostic methods which do not involve the use of probes penetrating into the hot plasma core. The following two sections deal with active techniques where the probes are either particle or photon beams. Finally, we discuss briefly those approaches that do not fall into the aforementioned categories or whose applicability is restricted to specific discharge conditions. In view of the large number of physical effects in magnetized plasmas and the consequential multitude of conceivable diagnostic schemes, it is hardly possible to pay due regard to all propositions. We concentrate, therefore, on those methods that have passed a feasibility test on a Tokamak installation and provided experimental information about the internal magnetic field or current density distribution. Those readers who are primarily interested in these results, may find a summary in the final chapter.

2. MAGNETIC FIELD STRUCTURE IN TOKAMAK EQUILIBRIA

Owing to the fact that the thermal velocity of the electrons in a Tokamak plasma is normally much higher than the drift velocity, direct measurements of the current density are extremely difficult. For this reason most diagnostic approaches resort to determining the internal magnetic field and make use of Ampère's law, $\mu_0 \mathbf{j} = \nabla \times \mathbf{B}$, in order to derive information on the current distribution. As sketched in Fig. 1, the magnetic field structure of a Tokamak consists of three components, namely (i) a strong toroidal field B_t produced by external coils, (ii) a poloidal field B_p brought about by the induced plasma current, and (iii) a small vertical field B_v to balance the outward hoop force due to plasma pressure and current. The relative ordering of B_v, B_p and B_t is given by $B_v \sim \varepsilon B_p \sim \varepsilon^2 B_t$, where $\varepsilon = a/R$ is the ratio of minor and major radii of the plasma torus. Because of symmetry in the toroidal co-ordinate, the

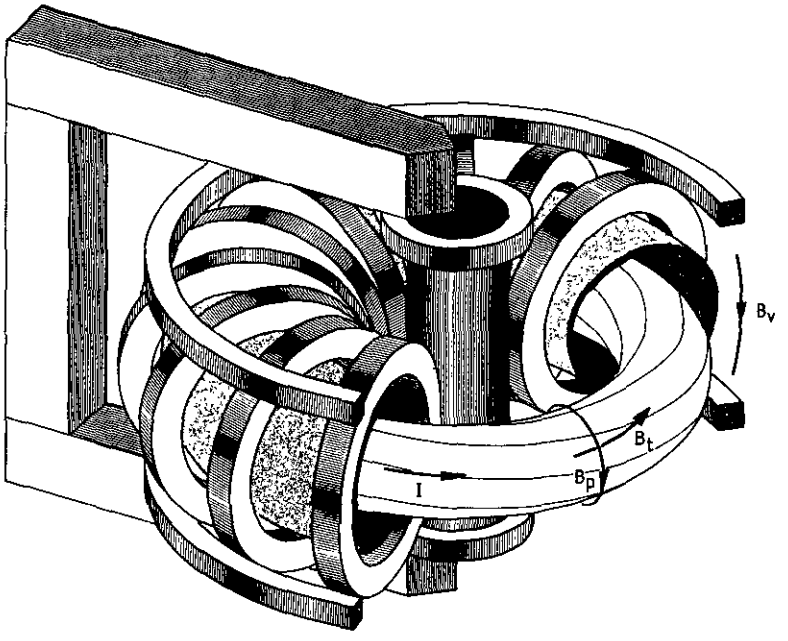

FIG. 1.—Schematic drawing of a Tokamak device.

magnetic field lines of the combined fields are helical and form a system of exact nested magnetic surfaces. The pitch of the field lines on each surface is characterized by the rotational transform ι or the safety factor $q = 2\pi/\iota$. For a slim torus with circular plasma cross-section and $\varepsilon \ll 1$, the magnetic surfaces come close to a set of concentric cylindrical tubes, and the safety factor as a function of the radius r takes on the simple form

$$q(r) = 2\pi/\iota(r) = (r/R)(B_t/B_p). \tag{2.1}$$

Under these conditions Ampère's law yields the following relations between the longitudinal current density j_t and the azimuthal field B_p:

$$j_t(r) = \frac{1}{\mu_0}\left(\frac{B_p(r)}{r} + \frac{dB_p}{dr}\right) \quad \text{and} \quad B_p(r) = \frac{\mu_0}{r}\int_0^r j(r')r'\,dr'. \tag{2.2}$$

Since the electrical conductivity of the plasma column is normally highest in the hot core, the current density $j_t(r)$ will be centrally peaked, and the induced field B_p and the safety factor q have a radial dependence as shown in Fig. 2. Magneto-hydrodynamic (MHD) stability conditions require that q at the plasma surface should be greater than one, and in practice most devices are operated with $q(a) \gtrsim 2$. For the plasma interior it has been argued that sawtooth activity would prevent the central value $q(0)$ from dropping significantly below unity, but this long-standing supposition has become questionable in recent years.

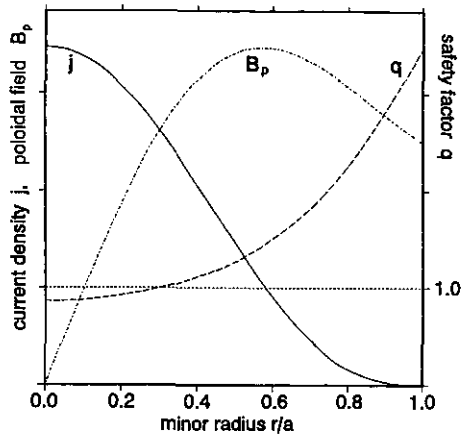

FIG. 2.—Illustrative radial profiles of current density j, poloidal magnetic field B_p and safety factor q.

Equation (2.2) and Fig. 2 reveal the basic problems encountered in a current profile determination via magnetic field measurements. The non-linear dependence of j_t on B_p and the characteristic shape of the field distribution lead us to divide the plasma cross-section into three zones with varying experimental demands.

(i) Close to the axis, B_p increases almost linearly with r, and the central current density is given by

$$j_t(0) = \frac{2}{\mu_0}\frac{dB_p}{dr}\bigg|_{r=0} \simeq \frac{2}{\mu_0}\frac{B_p(r_2)-B_p(r_1)}{r_2-r_1}. \tag{2.3}$$

The quantity of interest is the rate of change of B_p in the vicinity of $r = 0$, and the appropriate experimental technique is a differential measurement at two closely spaced positions on either side of the axis. Because of the smallness of B_p, systematic errors may be significant but can be tolerated as long as they are independent of r.

(ii) At intermediate radii, $r/a \simeq 0.5$, the slope dB_p/dr is small compared to B_p/r, and equation (2.2) reduces to

$$j_t(r) \simeq \frac{1}{\mu_0 r} B_p(r). \tag{2.4}$$

Here, the important parameter is the absolute value of B_p at well-known distances r from the axis. Since this region has the highest poloidal field, the attainable accuracy and the simple form of equation (2.4) permit a fair estimate of the local current density.

(iii) In the outer zone, $r/a \gtrsim 0.7$, there is little current flowing. Hence, in equation (2.2) the term B_p/r is nearly cancelled by dB_p/dr, and the poloidal field follows essentially a $1/r$-decay with some slight modifications due to the residual current density. Experimentally, these deviations are hardly detectable with reasonable precision, and one cannot expect to obtain detailed information on the far wing of the $j_t(r)$-profile.

The cylindrical model considered so far is only a crude approximation. A more realistic treatment of the magnetic field structure in Tokamak equilibria has to account for the toroidicity which introduces an outward shift of the plasma centre relative to the boundary. Furthermore, many modern devices feature non-circular plasma cross-sections ranging from simple vertical elongations to complicated bean shapes. A common property of all devices is the existence of nested toroidal surfaces which cannot be crossed by magnetic field lines. Hence, these surfaces may be labelled by the poloidal flux Ψ lying within them (see, e.g. WESSON, 1987). The poloidal magnetic field components are related to Ψ by

$$B_R = -\frac{1}{2\pi R}\frac{\partial \Psi}{\partial z} \quad \text{and} \quad B_z = \frac{1}{2\pi R}\frac{\partial \Psi}{\partial R}, \tag{2.5}$$

and the toroidal current density can be expressed as

$$j_t(R,z) = \frac{1}{\mu_0}\left(\frac{\partial B_R}{\partial z} - \frac{\partial B_z}{\partial R}\right) = -\frac{1}{2\pi\mu_0}\left[\frac{\partial}{\partial R}\left(\frac{1}{R}\frac{\partial \Psi}{\partial R}\right) + \frac{1}{R}\frac{\partial^2 \Psi}{\partial z^2}\right]. \tag{2.6}$$

The safety factor, which is defined as the number of times a magnetic field line winds the long way around the toroid divided by the number of transits the short way around, acquires the general form

$$q(\Psi) = \mathrm{d}\Phi/\mathrm{d}\Psi, \tag{2.7}$$

where Φ is the toroidal flux within a given surface.

For practical reasons it is generally impossible to map the vector field $\mathbf{B}_p(R,z)$ by measurements throughout the whole plasma cross-section, and the missing experimental data have to be substituted by detailed information on the shape of the flux contours $\Psi(R,z) = \text{const}$. The latter may be obtained, for example, by a tomographic reconstruction of the soft X-ray emission pattern (e.g. GRANNETZ and SMEULDERS, 1988) on the premise that the emissivity is constant on a flux surface. Numerical equilibrium calculations based on the Grad–Shafranov equation also provide the topology of the magnetic field structure, but the necessary input information and the computational effort are quite substantial (e.g. LAO *et al.*, 1985). In any case, support from other diagnostics will be indispensable in order to derive the current density with some confidence from poloidal field measurements.

3. INDIRECT AND PASSIVE METHODS

From the preceding discussion it should be obvious that there is no straightforward and universally applicable technique to measure the current density distribution. On the other hand, even rather elementary analyses of the plasma behaviour in terms of power balance or confinement properties can hardly be done without some knowledge of the j-profile. Therefore, the required information is often drawn from routinely available plasma parameters by invoking more or less verified relations with the sought-after current distribution. In this section, we list these indirect methods

together with the underlying assumptions and discuss a passive spectroscopic technique utilizing the radiation from intrinsic impurities.

3.1. *Electrical conductivity*

According to the theory of SPITZER and HÄRM (1953), the electrical conductivity of a fully ionized, uniform plasma along the magnetic field lines, $\sigma_\parallel$, is closely related to the electron temperature T_e:

$$\sigma_\parallel = \frac{9.696 \times 10^3}{\ln \Lambda} \frac{T_e^{3/2}}{\gamma(Z_{\text{eff}})}. \tag{3.1}$$

The dependence on the effective ion charge Z_{eff} is given by

$$\gamma(Z_{\text{eff}}) = Z_{\text{eff}} \left[0.29 + \frac{0.457}{1.077 + Z_{\text{eff}}} \right],$$

and the so-called Coulomb logarithm is calculated from

$$\Lambda = 1.09 \times 10^{14} \frac{T_e}{Z_{\text{eff}} \sqrt{n_e}}$$

(the numerical factors are valid for σ in amperes per volt per metre, T_e in electronvolts and n_e measured per metre cubed).

Applying these formulae, one may transform measured profiles of T_e, n_e and Z_{eff} into a conductivity profile and further into a current distribution

$$j_t(r) = \sigma_\parallel(r) U_l / 2\pi R \tag{3.2}$$

[here, r is not necessarily the radial distance from the plasma centre but a surface label which can be defined as $r = (S_\Psi/\pi)^{1/2}$ with S_Ψ being the cross-sectional area of a flux surface]. The procedure assumes that the average electric field on each surface is independent of r and is simply determined by the loop voltage U_l of the plasma torus. Furthermore, any non-classical contribution to the resistivity (e.g. small-scale turbulence) is ignored. The validity of these suppositions is generally checked by deducing a mean effective charge $\bar{Z}_{\text{eff}}$ from the total plasma resistance $\mathscr{R} = U_l / I_{\text{tot}}$ and comparing it with spectroscopic measurements of the impurity content. For a rough estimation one may put $\ln \Lambda \simeq 15$ and $\gamma(Z_{\text{eff}}) \simeq 0.5 \times \bar{Z}_{\text{eff}}$ and convert equation (3.1) into

$$\bar{Z}_{\text{eff}} \simeq 1.3 \times 10^3 \frac{U_l}{R I_{\text{tot}}} \int_0^a [T_e(r)]^{3/2} r \, dr. \tag{3.3}$$

Although agreement within the experimental uncertainties has been found in numerous studies, there remain objections to the theoretical model. In toroidal geometry with the magnetic field strength decreasing towards the outer edge, electrons can be

trapped in banana-shaped orbits and are thus excluded from carrying toroidal current. The resultant reduction of $\sigma_\parallel$ is usually taken into account by a so-called neo-classical correction to equation (3.1), and the average parallel conductivity on a flux surface is expressed as

$$\sigma_\parallel^{\mathrm{nc}} = g_T \sigma_\parallel. \tag{3.4}$$

The factor g_T is a complicated function of the electron collisionality, the inverse aspect ratio r/R, and the effective charge Z_{eff}. A widely used approximate form has been derived by HIRSHMAN *et al.* (1977). Although the inclusion of the neo-classical effect is still a matter of debate, recent investigations on JET (BARTLETT *et al.*, 1988) and TFTR (ZARNSTORFF *et al.*, 1990) appear to prove its significance, especially for large machines.

On the small devices ST and TFR attempts were made to determine the conductivity profile more directly by slightly modulating the loop voltage and measuring the plasma inductance $\tilde{L} = \tilde{U}_l/(\mathrm{d}\tilde{I}/\mathrm{d}t)$ as a function of frequency (DELLIS and HOSEA, 1973; TFR GROUP, 1975). The basic idea was to create a skin effect in the plasma and to adjust $\sigma(r)$ in the field diffusion equation such that the solution matched the observed frequency dependence. Recently, FUKAO *et al.* (1991) performed similar experiments on the tiny NOVA-2 Tokamak (minor radius 6 cm), where they imposed toroidal electric field pulses instead of sinusoidal oscillations. However, as in the earlier investigations, the achieved accuracy was rather poor and ruled the method out for detailed profile studies especially in hotter and larger plasmas.

3.2. *Equilibrium analysis*

Within the bounds of ideal magneto-hydrodynamics, the static equilibrium of plasma and field in a Tokamak is described by

$$(\nabla \times \mathbf{B}) \times \mathbf{B} = \mu_0 \nabla p \quad \text{and} \quad \nabla \cdot \mathbf{B} = 0, \tag{3.5}$$

where p is the kinetic pressure and μ_0 is the vacuum permeability. By making use of equation (2.5) and recognizing RB_t as being constant on a magnetic flux surface [i.e. writing $(2\pi/\mu_0)RB_t$ as a function F of Ψ], the conditions (3.5) can be reduced to a single differential equation for the poloidal flux Ψ, which is usually called the Grad–Shafranov equation (LÜST and SCHLÜTER, 1957; GRAD and RUBIN, 1958; SHAFRANOV, 1958):

$$R \frac{\partial}{\partial R}\left(\frac{1}{R}\frac{\partial \Psi}{\partial R}\right) + \frac{\partial^2 \Psi}{\partial z^2} = -4\pi^2 \mu_0 R^2 \frac{\mathrm{d}p}{\mathrm{d}\Psi} - \mu_0^2 F \frac{\mathrm{d}F}{\mathrm{d}\Psi}. \tag{3.6}$$

Its solution provides the equilibrium configuration of an axisymmetric toroid for specified functions $p(\Psi)$ and $F(\Psi)$ and appropriate boundary conditions.

For diagnostic applications one is faced with the inverse problem of finding a solution to equation (3.6), with arbitrary source functions, such that a given set of external magnetic measurements and other relevant experimental data is reproduced as well as possible. Mathematically, this problem is ill-posed, because a finite amount

of input information only warrants a specification of a finite set of integral characteristics. Nevertheless, considerable effort has been spent to develop a variety of numerical equilibrium reconstruction codes [for a recent example and a summary of previous work see LAO *et al.* (1990)]. The general approach is to choose parametrized classes of functions of Ψ and to determine the parameters in order to fit the measurements. However, especially for the core region, external magnetic data alone do not suffice to reconstruct the distribution of the plasma current. To this end further experimental information has to be included, such as the pressure profile, the plasma diamagnetism, the location of the $q = 1$ surface, or the value of the safety factor on the magnetic axis. Hence the quality of the deduced current density profiles depends heavily on the number and precision of the employed diagnostics in conjunction with a properly chosen parametrization. Furthermore, one has to keep in mind the basic assumption of a static, steady state, scalar pressure MHD equilibrium, which can be violated in many practical situations (as, e.g. in discharges with strong additional heating).

3.3. *Soft X-ray emission*

Most modern Tokamaks are equipped with X-ray imaging systems which allow one to view a poloidal plasma cross-section along a large number of collimated chords. A camera usually consists of a pinhole or slot aperture and an array of surface barrier diodes as illustrated in Fig. 3. Each detector measures the soft X-ray intensity in a broad spectral band ($1 \lesssim h\nu \lesssim 20$ keV) along its chord with a typical sampling frequency of 100 kHz or more. Owing to the high spatial and temporal resolution, these instruments are particularly well suited to detect rapid localized fluctuations of the soft X-ray emission that are frequently brought about by MHD instabilities. Since the latter tend to develop at "rational" magnetic surfaces (i.e. at surfaces with a safety factor $q = m/n$), a mode analysis of the fluctuations in terms of amplitude and phase relations among the chords can provide information on the q-profile (e.g. VON GOELER *et al.*, 1974).

More refined applications aim at reconstructing two-dimensional contour plots of the X-ray emissivity in order to reveal the structure and dynamics of MHD instabilities. For this purpose tomographic methods must be used which demand, in principle, chord-integrated information from all directions. With a single camera, sufficient data can only be obtained if the plasma rotates in the poloidal direction like

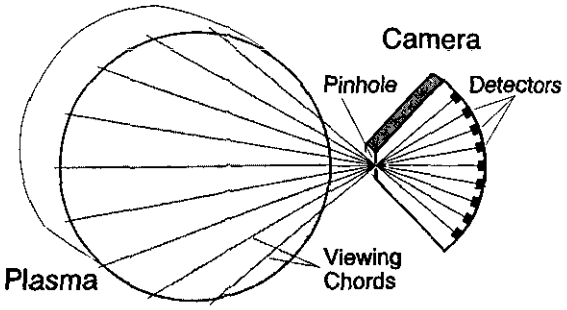

FIG. 3.—Schematic drawing of a soft X-ray pinhole camera.

a solid body with a frequency much higher than the rate of change of the observed structure (SAUTHOFF *et al.*, 1978). The analysis of very fast or non-oscillatory phenomena requires the use of several detector arrays arranged under different angles. The standard procedure is to describe the plasma emission in terms of Zernicke or Bessel polynomials of order ml for the minor radial dependence, and of angular harmonics $\sin m\theta$ and $\cos m\theta$. The angular expansion limit is determined by the number of arrays and hardly exceeds $m = 3$ for practical reasons. Consequently, the deduced X-ray emission pattern is not unambiguous, and the inclusion of additional views may completely change the result (JANICKI *et al.*, 1989).

Despite this restriction, soft X-ray tomography has become the prevalent method for studying the sawtooth phenomenon which is thought to be bound to the existence of a $q = 1$ surface and to details of the current density distribution in its vicinity. Extensive investigations on various Tokamak devices have led to rather divergent conceptions of the rapid sawtooth crash, ranging from a confirmation of Kadomtsev's total reconnection model (e.g. GRANETZ and CAMACHO, 1985) to strong support for Wesson's theory of a periodic quasi-interchange mode (e.g. EDWARDS *et al.*, 1986). For the most part, the inconsistency is certainly due to experimental and interpretive differences, but there remains also the question as to whether the contours of soft X-ray emissivity actually coincide with the magnetic surfaces in all circumstances. Unfortunately, this prerequisite is still barely more than a tacit assumption without a firm experimental basis.

3.4. *Polarization spectroscopy of intrinsic impurity lines*

More direct information on the magnetic fields can be obtained by exploiting the *Zeeman* effect on spectral lines emitted from intrinsic impurities. When atoms or ions are placed in a (weak) field B_0, each energy level is split into $(2J+1)$ sublevels with J being the total angular momentum number. The energy shifts are given by

$$\Delta E = Mg\mu_B B_0, \tag{3.7}$$

where M assumes values from $-J$ to $+J$ (g is the Landé-factor in case of pure LS-coupling, and μ_B is the Bohr magneton). Due to the energy splitting of the upper and lower levels of a transition, a spectral line disintegrates into a number of components whose polarization depends on the change in M and on the direction of observation relative to the magnetic field direction. In general, only transitions with $\Delta M = 0$ and $\Delta M = \pm 1$ are allowed. For $\Delta M = 0$ the radiation is always linearly polarized, whereas for $\Delta M = \pm 1$ the polarization varies from purely linear to purely circular when the line of sight is changed from perpendicular to parallel to the magnetic field. Thus, the relative content of circular polarization in these constituents of a spectral line is a direct measure of the magnetic field component along the direction of observation.

Polarization spectroscopy based on this effect has widely been used in astronomy to measure solar and stellar magnetic fields, and corresponding experimental and analytical techniques can be adapted to determine the poloidal field in a Tokamak plasma (FELDMAN *et al.*, 1984). In order to provide for a sufficient separation, $\Delta\lambda_B$, of the line components and to reduce the Doppler broadening, $\Delta\lambda_D$, due to thermal motion as much as possible, long-wavelength transitions of heavy species must be employed (the ratio $\Delta\lambda_B/\Delta\lambda_D$ scales as $\lambda_0 A^{-1/2}$, where λ_0 is the zero-field wavelength

and A is the atomic weight of the ion). The experimental procedure is to observe magnetic dipole transitions within the ground configuration of highly ionized stages of, e.g. Ti or Fe, which fall into the visible or near-ultraviolet spectral range. The line of sight is adjusted perpendicular to the toroidal field and is moved across a poloidal plane in a sequence of reproducible discharges in order to obtain a radial profile of the fractional circular polarization [for details of the registration technique see WRÓBLEWSKI *et al.* (1988a)].

Since the abundance of a particular ionization stage is highest in that region of the plasma where the electron temperature is approximately equal to the ionization potential, the emissivity of a certain transition is concentrated in a shell around the magnetic axis. Thus, a proper selection of transitions with fairly narrow radiating zones may already provide localized measurements, but detailed analyses require a precise knowledge of the volume emission profiles. In addition, the experimental data represent line-of-sight averaged results and need to be turned into local poloidal field values by means of appropriate inversion methods.

WRÓBLEWSKI *et al.* (1988b) have applied this technique on the TEXT Tokamak using a magnetic dipole transition of Ti XVII at 383.4 nm. The brightness distribution was rather broad and extended almost to the plasma edge which permitted them to determine nearly the full poloidal magnetic field profile on a shot-to-shot basis. For Ohmic discharges with densities of about 1.5×10^{19} m^{-3} and safety factors at the limiter between 2 and 3, they found significant discrepancies between the current profiles inferred from these measurements and those calculated from either classical or neo-classical resistivity. The q-profile appeared to be rather flat in the core region with a central value close to one. The experiment made great demands on the reproducibility of the Tokamak discharges, since each data point of the radial scan required five to ten shots in order to achieve acceptable signal-to-noise ratios.

Although the potential of polarization spectroscopy of intrinsic impurity lines is not yet fully exploited, a straightforward application in larger size devices seems difficult. On the one hand, the content of high-Z species is usually kept as small as possible, and on the other hand, the brightness of magnetic dipole transitions decreases rapidly with plasma density. These problems may, however, be circumvented if the radiation from heavy impurities is replaced by lines of lighter species excited by charge exchange with a high-energy neutral beam. Alternatively, one could use suitable spectral lines of the beam particles as described in the following section.

4. PARTICLE BEAM PROBE TECHNIQUES

The development of reliable particle beam systems has greatly enlarged the spectrum of potential magnetic field diagnostics, although at the expense of increased technical complexity. A number of concepts make use of particle beams to dope the plasma and to apply spectroscopic techniques for observing field-dependent radiation characteristics of the injected particles. Other approaches aim at determining the trajectories of the beam particles after they have been ionized and captured (or deflected) by the magnetic field. Out of the multitude of conceivable schemes we will discuss here only those methods that have been tested on Tokamak devices.

4.1. *Neutral lithium beam spectroscopy*

Lithium atoms combine several features which make them particularly attractive as doping species for diagnostic applications. Besides their low atomic weight, they

have a strongly allowed optical transition between the ground state and the first excited state (2^2P-2^2S; $\lambda = 670.8$ nm), and, furthermore, the Zeeman pattern of this line is essentially a simple triplet (provided that the magnetic field exceeds 1 T and the spin–orbit coupling breaks down). McCormick and co-workers were the first to utilize these properties for poloidal field measurements in the Pulsator Tokamak (McCormick *et al.*, 1977). They injected a mono-energetic neutral lithium beam into the plasma and observed the collisionally excited resonance line at right angles to the magnetic field. By means of a Fabry–Perot interferometer they isolated the central component of the Zeeman triplet and determined its plane of polarization which was oriented parallel to the local magnetic field direction at the intersection of the lithium beam and the line of sight. Thus they obtained the pitch angle γ of the field and were able to deduce the poloidal component $B_p = B_t \tan \gamma$. While these early measurements served more or less as proof of principle experiments, subsequent improvements of the lithium beam (in terms of current and energy) led to a routinely operable diagnostic system on the ASDEX machine (McCormick, 1986). It was mainly used to study the effects of lower-hybrid current drive (LHCD) on the internal magnetic field structure in low-density discharges. The safety factor on the magnetic axis was found to rise well above unity during LHCD, which explained the observed suppression of the sawtooth activity (McCormick *et al.*, 1987).

Probably the most advanced application of lithium beam spectroscopy has been devised by West and co-workers and implemented on the TEXT Tokamak (West, 1986). A schematic diagram of the set-up is shown in Fig. 4. It consists of a neutral beam system typically run at 95 keV with a current of 1 mA, and of a narrow-bandwidth cw dye laser whose output is directed collinearly with the Li beam into the torus along a major radius. The dye laser is tuned to match the central π component (but not the shifted σ components) of the Li resonance line, and the induced fluorescence is observed from the bottom by a multichannel detection system. The plane of polarization of the laser beam is caused to rotate continuously at 50 kHz. When it

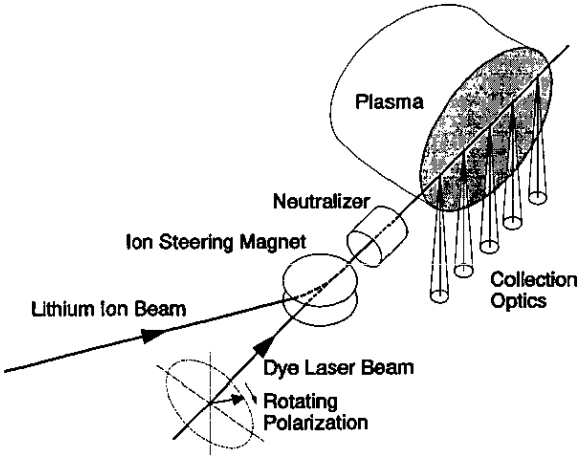

Fig. 4.—Schematic diagram of the lithium beam diagnostic in the TEXT Tokamak [after West (1986)].

points parallel to the local magnetic field, the π component can be excited, whereas no excitation occurs at right angles between the laser polarization and the field direction. Thus, the fluorescence signal exhibits a modulation at the frequency of the polarization rotation, and the phase is directly related to the tilt angle of the field lines.

In order to obtain adequate Li-beam penetration and to minimize collisionally induced fluorescence, measurements were performed for low-density discharges only. In Ohmically heated plasmas with $\bar{n}_e \leqslant 1 \times 10^{19}$ m^{-3} and low safety factors at the edge ($q_a \leqslant 3.5$), the axial value of q turned out to be significantly less than one ($q_0 = 0.8 \pm 0.1$). The result was corroborated by measurements in high-q_a discharges without sawtooth activity where q_0 was found to be greater than one (WEST *et al.*, 1987). Although these experiments appeared to be fairly conclusive, they were later called into question by spectroscopic investigations of a Ti XVII line on the same Tokamak under comparable discharge conditions (WRÓBLEWSKI *et al.*, 1988b; cf. Section 3d). Huang and co-workers tried to resolve the discrepancy by employing a mixture of both diagnostic techniques (HUANG *et al.*, 1990). They used the lithium beam of West and modified the spectroscopic detection system of Wróblewski to determine the fractional circular polarization of the Li I 670.8 nm line at various positions along the beam path. The analyzed data for Ohmically heated TEXT discharges with $q(a) = 2.0$ are shown in Fig. 5 together with a fitted curve and the q- and j-profiles derived from the latter. These results supported the measurements of

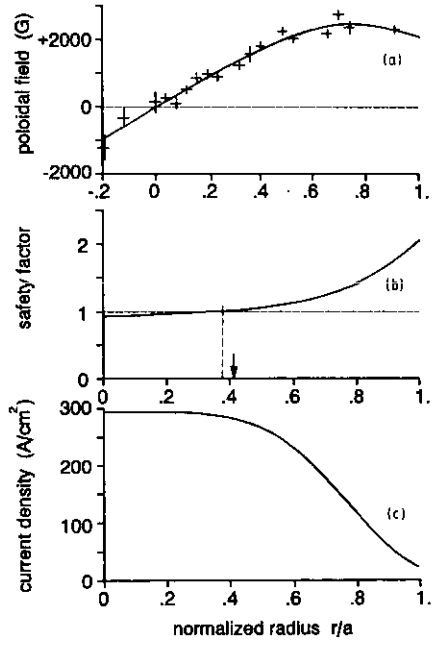

FIG. 5.—(a) Poloidal magnetic field profile measured in Ohmically heated TEXT discharges by means of polarization spectroscopy of injected lithium atoms. (b) Safety factor and (c) current density distribution derived from the fitted curve in (a). The arrow in (b) denotes the location of the soft X-ray sawtooth inversion radius [after HUANG *et al.* (1990)].

Wróblewski *et al.*, according to which the axial safety factor was close to unity in sawtoothing discharges.

A fundamental problem with neutral lithium beams is the large ionization cross-section and a resulting strong attenuation by the plasma (the characteristic depth to which the beam penetrates may be estimated from $\int n_e \, dl \lesssim 4 \times 10^{18}$ m^{-2}). For this reason both the experiments of West *et al.* and the subsequent investigations of Huang *et al.* suffered from very low signal levels which had to be improved by adding the data of many reproducible shots. In order to overcome this limitation and to enable corresponding measurements on larger devices, it has been proposed to replace the atomic beam by the ablation cloud of a high-speed lithium pellet. First experiments on Alcator C and TFTR (TERRY *et al.*, 1990) demonstrated the feasibility, but the achieved signal-to-noise ratios were too small to provide precise information about the plasma core region.

4.2. *Motional Stark effect on neutral hydrogen beams*

Atoms moving with a velocity $\mathbf{v}$ through a magnetized plasma experience in their rest frame an electric field $\mathbf{E}' = \mathbf{E} + \mathbf{v} \times \mathbf{B}$ which gives rise to a Stark splitting of the emission lines. For hydrogen the effect is linear with $\mathbf{E}'$ and results in a symmetric pattern of π and σ components with polarizations parallel and perpendicular to the electric field when viewed in the transverse direction. If one uses an energetic hydrogen beam, the electric field acting on the particles is completely determined by the $(\mathbf{v} \times \mathbf{B})$ term which can exceed 40 kV cm^{-1} for a beam energy of 50 keV and a magnetic field of 1.5 T. The spectral shift is much greater than the concomitant Zeeman splitting and permits a clear separation of components with orthogonal polarizations. In addition, the beam attenuation is tolerable also for larger plasma dimensions and densities, and an interference of thermal background line radiation is easily avoided due to the large Doppler shift of the spectrum emitted by the beam atoms.

The first measurements of the motional Stark effect on the deuterium Balmer α line ($\lambda = 656$ nm) were performed on JET by making use of the neutral beam injection system installed for plasma heating (BOILEAU *et al.*, 1989). The authors resolved the Stark pattern and determined the wavelength separation of the components with statistical errors of less than 1%. An evaluation of the poloidal magnetic field was, however, hindered by the unfavourable beam orientation and viewing line direction in conjunction with uncertainties about the flux geometry. These problems were overcome on the PBX-M Tokamak by Levinton and collaborators who employed a low-divergence diagnostic beam with variable injection angle (LEVINTON *et al.*, 1989). The injected power was typically 10 kW at an energy of 55 keV. Radial scans with a spatial resolution of 1–2 cm were obtained by changing the intersection of the beam and the fixed viewing axis from shot to shot. Instead of resolving individual Stark components of the H_α line, Levinton and his co-workers adopted spectroscopic techniques of the Li beam method and determined the direction of polarization of a manifold of Stark σ-components in order to derive the local pitch angle of the magnetic field lines. The required integration times were 40 ms for each data point of a radial scan. Taking into account the non-circular cross-section of the flux surfaces in PBX-M, the safety factor at the magnetic axis in typical Ohmic discharges was deduced to be $q(0) = 0.86 \pm 0.05$. This result, which represents an average over a sawtooth period,

was in agreement with the Fast Ion Diagnostic Experiment (FIDE) to be described in the next section.

Owing to the ready availability of suitable neutral hydrogen beams, the relative simplicity of the spectroscopic technique, and a fairly straightforward interpretation of the experimental data, q-profile measurements based on the motional Stark effect of hydrogen lines are likely to undergo a rapid development in the near future. From the DIII-D Tokamak first experiments have been reported (WRÓBLEWSKI and LAO, 1991) which indicate that the central q-value may be substantially smaller than one in highly elongated, double-null diverted discharges.

4.3. *Fast-ion orbits created by tangential neutral beam injection*

The trajectories of fast ions circulating in a Tokamak plasma depend on the internal magnetic fields and so can be used to determine the field structure. This approach was first applied by GOLDSTON (1978) on the Princeton ATC Tokamak and subsequently on the PDX device (GOLDSTON, 1982; MEYERHOFER *et al.*, 1985). Figure 6(a) shows the experimental set-up consisting of a tightly collimated neutral probe beam ($D^0, E_{inj} \leqslant 30$ keV, $P_{inj} \leqslant 10$ kW) and a neutral particle analyzer to detect the re-emitted charge-exchange neutrals. Both the beam and the detector sightline are ori-

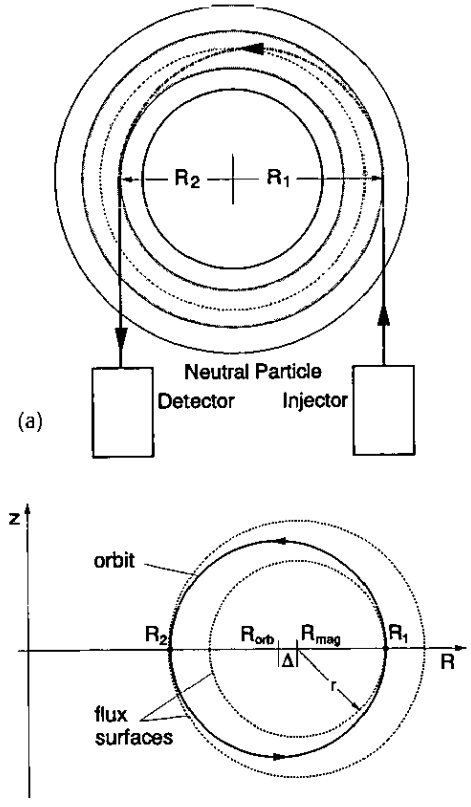

FIG. 6.—(a) Experimental set-up of the Fast-Ion Diagnostic Experiment (FIDE) for measuring the safety factor in the ATC and PDX Tokamaks. (b) Projection of the fast-ion orbits and magnetic flux surfaces in a poloidal plane.

ented in the horizontal midplane tangent to magnetic flux surfaces on opposite sides of the torus. To zeroth order, ions born at the injection point R_1 follow the helical magnetic field lines, and the finite pitch causes the ions to spread over a thin toroidal shell. This shell would coincide with a magnetic flux surface, if there were no drift motions. However, owing to the field line curvature and the field gradient along the major radius, there is a vertical drift which takes the particles away from the flux surface. The behaviour is illustrated in Fig. 6(b) for a beam aimed against the plasma current outside of the magnetic axis R_{mag}. As an ion travels from its birth place R_1 through the upper half of the plasma cross-section, it moves continuously towards larger minor radii. Below the horizontal midplane, the vertical drift takes the ion back to smaller minor radii until it eventually returns to its starting position. As a result, the orbit centre R_{orb} is displaced from the magnetic axis by a distance

$$\Delta = |R_{\text{mag}} - R_{\text{orb}}| = \frac{\sqrt{2m_i E_{\text{inj}}}}{q_i B_t} q(r), \tag{4.1}$$

where m_i and q_i are the ion mass and charge, respectively, and B_t is the toroidal field. In contrast to most other approaches, the observable quantity Δ is proportional to the safety factor $q(r)$, rather than the poloidal field, and remains therefore finite also in the plasma centre. While R_{orb} derives immediately from the tangency radii R_1 and R_2 of the probe beam and the detector sightline, the location of the magnetic axis is usually not well known. To circumvent this difficulty, advantage can be taken of the fact that the beam carries D^0 neutrals at energies of E_{inj}, $E_{\text{inj}}/2$, and $E_{\text{inj}}/3$. These components have different orbits and so allow one to eliminate R_{mag} in equation (4.1).

On the ATC Tokamak, corresponding measurements were performed with a single-sightline detector, and the necessary scan to determine the various orbits was done by changing the major radius of the plasma during a discharge. Furthermore, in order to discriminate against scattered and background particles, the injection voltage was modulated at 3 kHz. The central safety factor $q(0)$ was generally found to be larger than one but falling close to unity when the edge value $q(a)$ was lowered and sawtooth activity appeared. These results were in conflict with the current density profiles deduced from plasma resistivity which yielded significantly smaller values of $q(0)$. The discrepancy was attributed to a non-uniform distribution of Z_{eff} (GOLDSTON, 1978).

In subsequent experiments on PDX the detector was replaced by a ten-sightline neutral particle analyzer to provide sufficient spatial resolution without moving the plasma. The system was primarily employed to investigate the time evolution of the safety factor in the plasma centre during the initial phase of current penetration. As expected, the central q value decreased smoothly with falling $q(a)$, but in contrast to the ATC results, it continued to drop down to 0.6 ± 0.4 as the plasma current was held constant (GOLDSTON, 1982). A recent reappraisal of the experimental conditions and uncertainties in the PDX measurements corroborated this finding (KUGEL *et al.*, 1988). The study also revealed a number of critical points for potential application on PBX-M at higher densities and additional heating beam powers, among which the energy of the diagnostic beam and the magnetic shielding of the detector against stray fields appeared to be the most significant.

4.4. *Deflection of heavy ion beams*

Heavy ions injected perpendicular to the plasma current experience a $\mathbf{v} \times \mathbf{B}$ force which is primarily determined by the large *toroidal* field component B_t. If the energy and mass of these ions are chosen such that their Larmor radius is larger than the plasma radius, they will not be captured in the plasma but traverse it on a curved path. The trajectory stays close to the plane of injection, but due to the small *poloidal* field component B_p there is a slight deviation in the toroidal direction. Since the exact emerging point is determined by an integral over the path of the total field, the spatial field variation can, in principle, be deduced by sweeping the beam across the plasma and performing a rather involved integral deconvolution.

Experimentally, it is more appropriate to observe an array of secondary beams which are created by further ionization of the injected particles all along the primary trajectory (JOBES and HICKOK, 1970). Because the secondaries double their charge, they have half the Larmor radius of the parent ions. Hence they depart from the main beam and their escape position on the plasma surface is directly related to the birth position. A set of detectors, which is suitably placed to intercept secondaries from selected points of the main path, can thus provide sufficient information to reconstruct the poloidal field distribution from the toroidal displacements of the respective orbits (see Fig. 7). In practice, however, the uncertainties accumulating from various field perturbations turned out to be quite substantial (JOBES, 1975). Exploratory measurements in the small ST Tokamak using Cs^+ ions of some 10–50 keV and beam currents of a few micro amperes were rather inconclusive and yielded barely more than a rough confirmation of estimates derived from plasma conductivity. Furthermore, a straightforward adaptation to larger plasmas and higher fields would be hindered by the need for extreme ion energies.

5. PHOTON BEAM PROBE TECHNIQUES

Except for an early attempt based on microwave propagation, other photon beam probe techniques for magnetic field measurements have not been developed as independent instrumentations, but a number of proven systems designed for different diagnostic purposes has been upgraded to take on the additional task. One of these approaches is linked to the well-established Thomson scattering technique and makes use of the fact that the scattered light spectrum splits up into a multitude of discrete

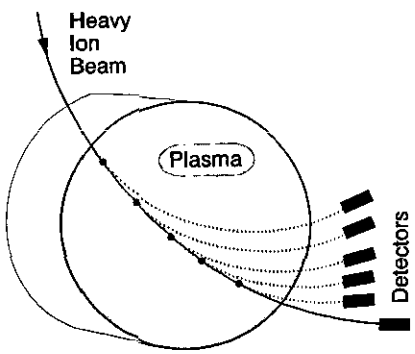

FIG. 7.—Primary and secondary orbits for heavy ion beam probing.

lines when the scattering vector is oriented exactly perpendicular to the local magnetic field. Another scheme exploits the Faraday effect on far-infrared laser beams and takes advantage of the technical maturity of corresponding multi-channel interferometers. The latter method has been pursued fairly actively in recent years, and several instruments have been constructed and operated on various medium-sized and large Tokamaks.

5.1. *Harmonic generation by microwave beams*

According to the theoretical analyses of FIDONE *et al.* (1971), a microwave beam traversing a magnetized plasma generates harmonic waves if it encounters a region where the incident frequency ω_{in} matches the upper hybrid frequency

$$\omega_{uh} = \sqrt{\omega_{ce}^2 + \omega_{pe}^2} \tag{5.1}$$

(with $\omega_{ce} = eB/m_e$ being the electron cyclotron frequency and $\omega_{pe} = (e^2 n_e/\varepsilon_0 m_e)^{1/2}$ the plasma frequency). The harmonic waves are plane-polarized at right angles to the magnetic field direction in the resonance layer and thus carry information on the local pitch angle. Cano and co-workers used this property to determine the poloidal field distribution in the ST Tokamak (CANO *et al.*, 1975). They launched a microwave beam from the inboard side of the torus into the plasma and detected the second harmonic at the outboard side diametrically opposed to the emitting horn. The receiving system included a sensitive polarimeter to measure the tilt angle of the electric field of the harmonic wave relative to the horizontal midplane. The frequency $2\omega_{in}$ was high enough to ignore birefringent effects of the plasma. Hence the direction of polarization corresponded directly to the field line direction at the place of origin. The location of the resonance layer was calculated from equation (5.1) using the known toroidal field distribution $B_t(R)$ and the electron density profile $n_e(R)$ deduced from Thomson scattering measurements. By varying the level of B_t for a constant incident frequency, the layer was moved along the major radius and the poloidal magnetic field was obtained as a function of R. The results provided a reasonable indication of the profile shape, but the error bars were too large to contrast the data quantitatively with those derived from plasma conductivity.

Apart from experimental difficulties (as, e.g. de-polarization due to reflections from metallic surfaces) and uncertainties of the position of the resonance layer, the technique is limited to conditions where (i) the upper hybrid resonance is accessible and (ii) the harmonic wave can leave the plasma essentially unperturbed. Mainly for these reasons the method has not been adopted on other devices.

5.2. *Incoherent Thomson scattering*

Virtually all Tokamak facilities are equipped with Thomson scattering systems for routine measurements of the electron density and temperature. The usual arrangement of the laser light source and the collection optics is such that the wave vector $\mathbf{k}_o$ of the incident beam and the vector $\mathbf{k}_s$ of the scattered wave are orthogonal to each other and to the direction of the plasma current. Since the observed spectrum corresponds to the projection of the electron velocity distribution on the scattering vector $\mathbf{k} = \mathbf{k}_s - \mathbf{k}_o$, this geometry selects velocity components along a minor radius and

excludes any contribution of the drift velocity $\mathbf{v}_D$ of the current-carrying electrons. By changing the optical set-up such that the difference vector $\mathbf{k}$ has a major component parallel to the plasma current, it is, in principle, possible to access $\mathbf{v}_D$ and to determine the current density $\mathbf{j} = en_e\mathbf{v}_D$. However, for typical plasma conditions the electron drift velocity is much less than the mean thermal velocity and leads only to a minute shift of the detected spectrum. Although the technique has been used successfully on small Tokamaks (ALLADIO and MARTONE, 1977; BARTH, 1989), its applicability to plasmas with electron temperatures in excess of a few hundred electronvolts seems questionable. Here the spectral shift will be masked by relativistic asymmetries of the scattered light spectrum, and non-thermal features are likely to cause further distortions. In addition, contributions from the ions to the total current and bulk rotations of the plasma torus would have to be measured independently.

A more promising modification of Thomson scattering systems is aimed at detecting characteristic modulations of the spectrum which occur when $\mathbf{k}$ is at right angles to the magnetic field $\mathbf{B}$ in the scattering volume. In this case, the effective velocity along $\mathbf{k}$ is given by a sinusoidal oscillation of the electrons due to the gyration around the field lines. Hence the scattered light from each electron has a Doppler shift that varies in time at the cyclotron frequency ω_{ce}. Consequently, the observed spectral distribution consists of a series of peaks which are separated by ω_{ce} and bounded by an envelope of width $2kv_e$ (with v_e being the electron thermal velocity and k denoting the absolute value of $\mathbf{k}$; see Fig. 8). These peaks would be smeared out, however, if the Doppler shifts due to thermal motion parallel to the field were as large as ω_{ce}. Given a small angle ψ between $\mathbf{k}$ and the perpendicular to $\mathbf{B}$, the width of the peaks is $2kv_e \sin\psi$. Thus, the existence of the modulation means that $\psi \lesssim \omega_{ce}/(2kv_e)$, which amounts to one degree or less for common Tokamak parameters. So the mere observation of a periodic structure in the scattered light spectrum provides precise information on the local magnetic field direction.

In return for the inherent accuracy, the experiment makes great demands on a proper lay-out and meticulous installation of the optical arrangement. For a customary 90° scattering system employing a ruby laser to probe a plasma of $T_e \simeq 1$ keV in a field of about 2 T, the number of peaks within the e-folding points of the Gaussian envelope exceeds 1300, and the scattered intensity in each of these harmonics is of the order of one photon only. Obviously, a technique to superimpose the separate peaks has to be used, and the width of the envelope has to be decreased by choosing a

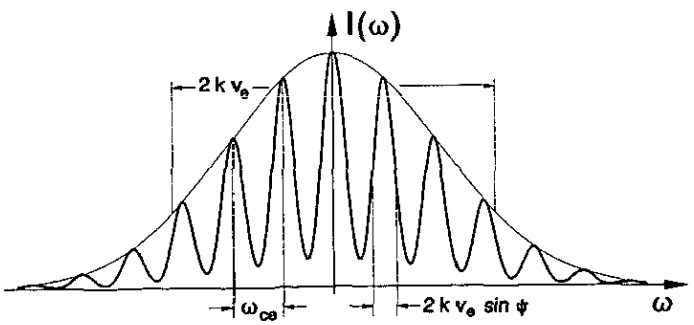

FIG. 8.—Shape of the scattered light spectrum for $\mathbf{k}$ almost perpendicular to $\mathbf{B}$.

smaller scattering angle (i.e. by changing over to forward scattering). The first problem can be solved by means of a Fabry–Perot interferometer whose free spectral range is adjusted to match the electron cyclotron frequency (SHEFFIELD, 1972). Such a device rejects light at frequencies in-between the harmonics and thus reduces the intensity of a smooth spectrum, whereas a modulated spectrum will pass without attenuation. Since the finite acceptance cone of the collection optics covers a whole range of angles ψ between $\mathbf{k}$ and the perpendicular to $\mathbf{B}$, the output pattern of the interferometer will exhibit a bright zone corresponding to maximum modulation at $\psi \simeq 0$. The second requirement, namely decreasing the width of the Gaussian envelope by reducing the scattering angle, inevitably involves an extension of the scattering volume along the laser beam and hence a deterioration of the spatial resolution. Besides that, the pitch angle variation within the enlarged volume smears out the modulation in the wings of the spectrum. These limitations as well as further practical constraints have been discussed in detail by CAROLAN (1977).

As yet the only successful demonstration of the technique has been accomplished on the DITE Tokamak (FORREST *et al.*, 1978). The authors directed a ruby laser beam vertically through the plasma and observed the light scattered under 30° at various positions along the beam path by a set of prisms. The system accuracy was estimated to yield the magnetic field line inclination to within 0.15° and to provide the corresponding safety factor with an uncertainty of 5%. Values for q of less than one were found in the central region of the plasma.

Clearly, the experimental demands are extremely difficult to satisfy and do not recommend the method for routine use on major fusion devices. Nevertheless, the technique lends itself to occasional precision measurements in order to corroborate the results of other magnetic field diagnostics and to clarify details of the q-profile under specific discharge conditions. Therefore, serious consideration has been given to a pertinent extension of the Thomson scattering system on TFTR (BRIZARD *et al.*, 1986), and the existing single point scattering apparatus on JET is presently being modified to allow a multipositional determination of the poloidal field with an estimated accuracy of about 10% (CAROLAN *et al.*, 1990).

5.3. *Faraday effect on far-infrared laser beams*

The application of far-infrared polarimetry for magnetic field measurements goes back to a proposal of DEMARCO and SEGRE (1972) and is schematically shown in Fig. 9. Plane-polarized waves traversing a poloidal cross-section normal to the plasma current experience a phase shift $\Delta\varphi$ and a rotation α of their plane of polarization according to

$$\Delta\varphi(x) = r_e\lambda \int_L n_e \, dz \quad \text{and} \quad \alpha(x) = \frac{er_c}{2\pi c m_e} \lambda^2 \int_L n_e B_{p\parallel} \, dz, \tag{5.2}$$

where λ is the vacuum wavelength, $r_c = 2.818 \times 10^{-15}$ m is the classical electron radius, n_e is the electron density, and $B_{p\parallel}$ denotes the magnetic field component parallel to the beam path. Both quantities $\Delta\varphi$ and α can be measured simultaneously by combining an interferometer with a polarimeter in a variety of conceivable schemes. A technique which fits particularly well into the optical system of customary phase-modulated

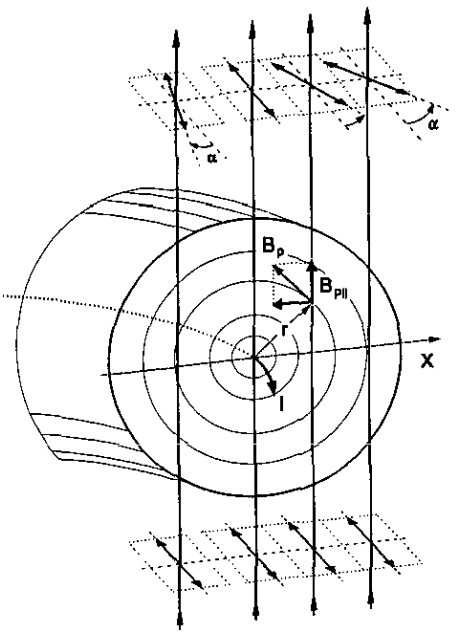

FIG. 9.—Principle of poloidal magnetic field measurements by far-infrared polarimetry.

interferometers has been proposed by JACOBSON (1977) and VÉRON (1979). Its basic idea is to replace the beam combiner of the interferometer by a polarizer and thereby split off that component of the probing wave which has acquired a polarization perpendicular to the initial one. By mixing it with a local oscillator, a beat signal is obtained with an amplitude approximately proportional to the Faraday rotation angle α. The local oscillator is provided by the interferometric reference beam which is frequency-shifted to enable phase modulation. Based on this scheme a multi-channel interferometer/polarimeter has been constructed and routinely operated on the TEXTOR Tokamak (SOLTWISCH, 1983) and subsequently on JET (BRAITHWAITE *et al.*, 1989). The appropriate wavelengths of the probing beams are in the far-infrared regime ($0.1 \lesssim \lambda$ [mm] $\lesssim 0.5$) and result from a compromise between sufficiently large values of $\Delta\varphi$ and α and small perturbing effects (such as beam deflection due to density gradients and elliptical polarization caused by transverse magnetic field components). A more detailed description of the principles together with design considerations and technical aspects of the apparatus was given by SOLTWISCH (1986a).

In order to determine local values of n_e and B_p, the full profiles $\Delta\varphi(x)$ and $\alpha(x)$ have to be known and assumptions have to be made about inherent symmetries of the sought-after distributions. For the simple case of a cylindrical plasma column, $B_{p\parallel}$ reduces to $(x/r)B_p(r)$, where x is the chord distance from the centre, and the Faraday rotation angle becomes

$$\alpha(x) = \frac{er_e}{\pi c m_e} \lambda^2 \int_0^{\sqrt{a^2-x^2}} (x/r) n_e B_p \, dz. \tag{5.3}$$

Interpreting (x/r) and n_e as weight functions along the beam path, one notices that both of them have a maximum in the equatorial midplane and fall off towards the plasma boundary, thus emphasizing the information on B_p gathered near $z = 0$ and attenuating the influence of the outer plasma regions. It is this localization which makes it possible to draw fairly accurate information also on the plasma centre where the poloidal field is rather small.

A detailed reconstruction of the field distribution has to take into account the exact shape and shift of the magnetic flux surfaces as well as a number of spurious effects on the experimental data. Instrumental deficiencies (as, e.g. imperfections of the optical components or non-linearities of the signal detection and processing system) can be circumvented by a careful absolute calibration, whereas plasma-induced perturbations are more difficult to handle. For example, appropriate account of a slight elliptization of the probing wave polarization due to transverse magnetic fields within the plasma can be made only by iteration since this effect depends on the amount of Faraday rotation and hence on the sought-after poloidal field distribution. The same is true for the shape and shift of the flux surfaces which are related by equilibrium conditions to the initially unknown current density profile. A feasible way to treat these complications is to use trial functions for the current distribution, determine the corresponding surface structure by equilibrium calculations, evaluate the plasma-induced polarization changes in hypothetical probing beams, and follow these beams through the (imperfect) optical set-up and detection system. Thus "theoretical" signals are created which have to be matched successively to the experimental data as closely as possible.

As with all line-integrated information, the limited number of probing chords and the finite signal-to-noise ratios leave some latitude for the evaluation of the local data. A statistical error analysis performed for the nine-channel polarimeter installed on TEXTOR indicates that the percentage error of B_p is lowest at intermediate radii (about $\pm 5\%$ within $0.4 \leqslant r/a \leqslant 0.6$) and increases rapidly towards the centre and the edge of the plasma column. For the central current density j_0, which is proportional to $(\partial B_p/\partial r)_{r=0}$, an accuracy of $\pm 15\%$ can be obtained by slowly moving the plasma across the central probing chord during quasi-stationary discharge conditions and thereby measuring the slope $\partial\alpha/\partial x$ of the Faraday rotation profile at its zero-crossing (as mentioned before, the rotation angle yields fairly localized information on B_p near the plasma centre, and there is a close relation between $\partial\alpha/\partial x$ and $\partial B_p/\partial r$). Of course, these estimates hold only for smooth profiles. Spatial structures like small indentations can only be resolved if their extension is larger than the spacing of the probing chords or if they can be moved without alteration across a fixed beam.

Extensive polarimetric measurements on a large number of Ohmic TEXTOR discharges have shown that there exists a unique current density profile to which a fairly broad variety of experimental distributions can be fitted by displaying j in units of $B_t/(\mu_0 R)$ and r in units of $(\mu_0 RI/B_t)^{1/2}$ (SOLTWISCH *et al.*, 1986b; see Fig. 10). Since the normalization factors depend only on external Tokamak parameters, the reduced profile should have a universal character independent of a given device for a certain range of plasma conditions whose limits have not yet been fully explored. The central value of this universal distribution corresponds to an axial safety factor q_0 of about 0.75 representing an average over a sawtooth period. The variation of q_0 during a sawtooth cycle has been determined by making use of the high reproducibility of the

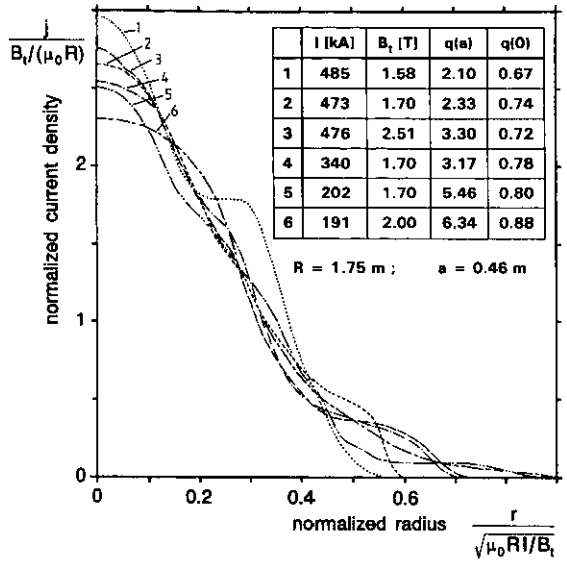

FIG. 10.—Superposition of normalized current density profiles measured in a variety of quasi-stationary sawtoothing Ohmic discharges in TEXTOR (see insert). In reduced coordinates the profiles resemble roughly a universal profile (after SOLTWISCH *et al.*, 1986b).

sawtooth phenomenon under appropriate quasi-stationary discharge conditions and applying coherent signal averaging techniques. It was found that j_0 (and hence q_0) undergoes a sawtooth-like modulation with an amplitude of $\lesssim 8\%$ of the average value (SOLTWISCH, 1988). Similar results were obtained on JET where improved signal-to-noise ratios of the polarimetric data and sawtooth periods much in excess of the temporal resolution permitted the analysis of individual sawtooth events (O'ROURKE, 1991).

Considering the relatively broad range of applications and results, far-infrared polarimetry has reached a fairly advanced stage compared to most other magnetic field diagnostics. There remains, however, the basic problem of unfolding the line-integrated data which cannot be done without a thorough knowledge of the electron density profile and the magnetic flux pattern. Hence, for plasmas with strongly shifted or non-circular flux surfaces, this method depends more than other approaches on additional information from, e.g. soft X-ray tomography or extensive equilibrium code calculations.

6. MISCELLANEOUS TECHNIQUES

Most of the schemes considered so far have been put into practice as more or less self-contained diagnostic instruments. In addition, there exist some techniques which are intrinsically linked to certain auxiliary equipment on a Tokamak device and take advantage of some fortuitous side-effects. In particular, the injection of solid hydrogen or deuterium pellets for plasma fuelling offers the possibility to draw information on the q-profile from the structure of the ablation cloud and from a characteristic behaviour at the $q = 1$ surface. Also, the equipment installed for wave heating on some machines can be used to excite a spectrum of Alfvén waves whose properties

depend on the safety factor profile. Both approaches have been used on various Tokamaks.

6.1. *Ablation pattern of injected hydrogen and deuterium pellets*

Pellets of frozen hydrogen or deuterium are frequently injected into Tokamak plasmas in order to modify the temperature and density profiles and to study the feasibility of refuelling a fusion rector. A common observation in these experiments is a modulation of the visible light and X-ray emission from the ablation zone as the pellet penetrates into the plasma core and crosses the magnetic surfaces. Photographic pictures of the pellet trajectories exhibit dark and bright streaks which extend toroidally within the ablation cloud and make a small angle with respect to the toroidal direction. Drawin and co-workers were the first to relate this inclination to the local pitch of the magnetic field lines and to analyze the radial-dependent tilt angles in terms of the rotational transform or safety factor profiles [TFR GROUP (1986); see also TFR GROUP (1987) for a reproduction of photographs and a comprehensive description of the experiments]. Since many of the pellets did not reach the plasma centre, the bulk of the measurements performed in TFR were confined to minor radii $r/a \gtrsim 0.4$. In this range the experimental q-values agreed well with theoretical q-profiles which were calculated from the Spitzer electrical conductivity using plasma parameters measured a few milliseconds before pellet injection. It is worth noting, though, that the striations did not always follow straight lines, with irregularities appearing predominantly in the region of $q \simeq 2$ and, for sufficiently deep pellet penetration, also at $q \simeq 1$. Moreover, measurements up to the magnetic axis in the TEXT Tokamak (DURST *et al.*, 1988) yielded central q-values significantly below 0.5 which were, however, not corroborated by the lithium beam probe technique employed on quite similar discharges (cf. Section 4.1). These incongruous results and a still incomplete understanding of the mechanism that causes the striations to align along the magnetic field lines cast some doubt on the general applicability of the method.

A characteristic feature of the ablation process is a pronounced reduction of the H_α line intensity as the pellet crosses the $q = 1$ surface (the latter is usually inferred from the inversion radius of sawteeth observed in the soft X-ray emission before pellet injection). GILL *et al.* (1989) and, in more detail, PÉGOURIÉ and DUBOIS (1990) have interpreted this phenomenon as being due to an annular region with very low magnetic shear in the vicinity of the $q = 1$ radius. The conclusion is based on the conception that the ablation of the pellet and the excitation of evaporated hydrogen atoms are caused by plasma electrons moving along the magnetic field lines with a speed much higher than the pellet velocity. Hence the pellet is regarded as quasi-motionless relative to the plasma, and almost all electrons on a non-rational q-surface can interact with the ablation cloud and give rise to a strong collisional excitation of the H_α line. On rational surfaces, in contrast, the flux tubes close on themselves, thus restricting the number of electrons which can hit the pellet. Flux tubes winding around the $q = 1$ surface are particularly short and contain only a small energy reservoir available for ablation and collisional excitation. If, in addition, the variation dq/dr is small in this region, the argumentation applies to a whole section of the pellet trajectory, rather than a single point, and explains the strong drop in the H_α line intensity.

For a measured width Δ of the dark zone and a calculated diameter d_c of the

ablation cloud, the local shear at the $q = 1$ surface can be estimated from geometrical considerations. The idea is that adjacent surfaces become sufficiently "irrational" to produce strong H_α emission if their rotational transform deviates from 2π by more than d_c/r_1 or, in other words, if an electron starting at the pellet does not encounter the cloud again after one toroidal transit. This model, then, leads to

$$\left.\frac{dq}{dr}\right|_{r_1} = \frac{d_c}{\pi r_1 \Delta}, \tag{6.1}$$

where r_1 is the $q = 1$ radius. Using this formula and inserting typical values measured in JET, GILL *et al.* (1989) obtained $dq/dr \simeq 4 \times 10^{-2}\ m^{-1}$. A more elaborate analysis by PÉGOURIÉ and DUBOIS (1990), who took into account possible effects of island formation and plasma rotation, produced similar results. For a smooth q-profile varying as $q_0(1+\alpha r^2)$, the low shear close to $q = 1$ would correspond to a central safety factor $q_0 \simeq 0.99$. However, such an extrapolation is questionable because the q-profile may very well have a local flattening in the region of $q = 1$ and fall substantially below unity in the plasma centre as was observed in the TEXTOR Tokamak (SOLTWISCH *et al.*, 1986b).

6.2. *Excitation of resonant Alfvén waves*

Alfvén waves are low-frequency plasma oscillations perpendicular to the magnetic field lines which propagate along **B** with a phase velocity $v_A = B/\sqrt{\mu_0 \rho}$ (with ρ being the mass density). Since these waves provide a possible means for the additional heating of a Tokamak plasma, their properties have been studied in considerable detail. Notably on the TCA device dedicated experiments were carried out by using a special antenna system in order to excite different mode structures (e.g. BEHN *et al.*, 1984). For a fixed driving frequency ω and imposed toroidal and poloidal mode numbers (n, m), Alfvén resonances occurred at those locations where $\rho(r)$ and the safety factor profile $q(r)$ had appropriate values in order to satisfy the condition

$$\omega = \frac{B_t/R}{\sqrt{\mu_0 \rho(r)}}\left(n + \frac{m}{q(r)}\right). \tag{6.2}$$

(Strictly speaking, this expression is a large-aspect-ratio cylindrical approximation where B_t denotes the toroidal field strength and R is the major radius; in addition, the ion-cyclotron frequency ω_{ci} is assumed to be much less than ω.) The position of the resonance layer could be determined from strong density fluctuations caused by kinetic effects in this region. Experimentally, a phase-contrast imaging interferometer served to detect the radius r_A at which these fluctuations appeared. Thus, in the case of a well-known mass density distribution, the measured dependence $r_A(\omega)$ for a given (n, m) mode would suffice to deduce the q-profile.

WEISEN *et al.* (1989) used this approach on TCA, although in a refined manner. In order to circumvent a precise determination of $\rho(r)$, they excited successively the $(n, m) = (1, 1)$ and $(2, 0)$ resonances in a sequence of identical discharges. The driving frequency was held constant, and the resonance layers were swept across the plasma radius by a continuous increase of the density which occurred automatically during

the excitation of the Alfvén waves. Then, writing the mass density as $\rho(r) = \rho(0) \times S(r)$ and assuming the profile shape $S(r)$ as being independent of a particular mode, the resonance conditions (6.2) for $(n, m) = (1, 1)$ and $(2, 0)$ were combined to yield

$$q(r) = [2[\rho_{11}(0)/\rho_{20}(0)]^{1/2} - 1]^{-1}. \tag{6.3}$$

So the safety factor at a certain radius r_A could be inferred from the central values $\rho_{nm}(0)$ which were required to place the $(1, 1)$ and $(2, 0)$ resonance layers at that position. Although the mass densities were unknown, their ratio ρ_{11}/ρ_{20} was obtained from electron line-density measurements under the assumption that the plasmas always had the same effective ion mass. For discharges with well-developed sawtooth activity it was found that both resonances occurred in the plasma centre at exactly the same density. This observation led to the conclusion that the axial safety factor $q(0)$ had to be very close to unity. Furthermore, a flat part of the reconstructed q-profile extended to the sawtooth inversion radius (as determined from soft X-ray measurements), and the outer portion extrapolated reasonably well to the safety factor at the plasma surface. Examples for different discharge parameters are shown in Fig. 11 where the subfigures (a)–(c) represent a current scan with vanishing sawtooth activity for $q(a) \gtrsim 5$. The uncertainties arising from the exact positions of the resonance layers and from the corresponding line-averaged electron densities were small in the centre but increased rapidly towards the edge. However, systematic errors due to a cylindrical approximation of the resonance condition and a possible excitation

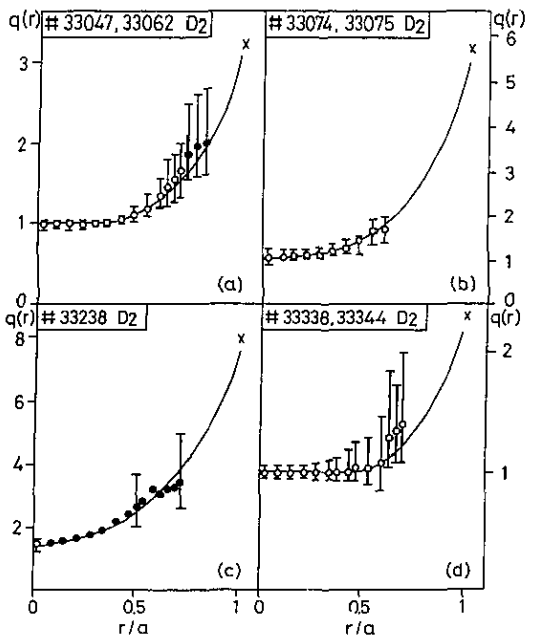

FIG. 11.—Safety factor profiles measured in TCA for (a) $B_t = 1.51$ T, $I_p = 125$ kA, (b) $B_t = 1.51$ T, $I_p = 70$ kA, (c) $B_t = 1.51$ T, $I_p = 50$ kA, and (d) $B_t = 1.16$ T, $I_p = 135$ kA (after WEISEN *et al.*, 1989).

of higher-order modes in toroidal geometry have not been discussed for these experiments.

DESCAMPS *et al.* (1990) determined the central q-value in the TEXTOR device by making use of a different feature of Alfvén waves in Tokamak plasmas. While the condition (6.2) for the excitation of a local (n, m) resonance requires a minimum driving frequency $\omega_{\min}$ for given profiles $\rho(r)$ and $q(r)$, discrete peaks in the antenna loading appear already at frequencies slightly below $\omega_{\min}$. These narrow resonances are global eigenmodes of the Alfvén wave due to finite ω/ω_{ci} effects in a non-uniform plasma. Their frequency separations from $\omega_{\min}$ depend sensitively on the spatial distributions of mass density and safety factor and so offer a further possibility to gain information on the q-profile. In a rather simple experimental set-up, Descamps and his co-workers fed one of the antennae designed for ion-cyclotron-heating experiments with a 400 W broad band generator and swept the frequency from 0 to 3 MHz during the quasi-stationary phase of Ohmic discharges. An electrical dipole located 30° away in the toroidal direction served to register the poloidal field component and to detect the discrete Alfvén eigenmodes. A plot of the field amplitudes versus frequency showed a series of distinct peaks which could be related to corresponding (n, m) modes by comparison with code calculations. Although, in accordance with theoretical predictions, modes with $|n+m| = \text{const}$ were nearly degenerate, some of the resonances having the same $|n+m|$ value were clearly split into individual peaks. The measured frequency separations were well reproduced by model calculations assuming a q-profile with a central value of 0.7, whereas $q(0) \simeq 1$ was far beyond the bounds of probability. This result was in agreement with polarimetric measurements on very similar discharges in TEXTOR as described in Section 5.3.

7. SUMMARY OF THE EXPERIMENTAL RESULTS

From the preceding discussion it should be clear that most of the employed techniques to measure current densities and magnetic fields in Tokamak devices have barely passed the exploratory stage of development. Consequently, many of the reported results stem from tests of the conceptual and practical feasibility rather than from systematic studies of certain physical issues. This situation is, for a large part, due to the discovery of the sawtooth phenomenon (VON GOELER *et al.*, 1974) and to Kadomtsev's theory of the underlying mechanism (KADOMTSEV, 1975), which was widely accepted until the mid 1980s. Since the sawtooth activity was believed to pin down the axial safety factor close to unity, it became a simple matter to calculate the central portion of the current density distribution and to construct the wings of the profile beyond the $q = 1$ radius in such a way that (i) $j(r)$ decayed monotonically to zero at the plasma edge and (ii) the integral $2\pi \int_0^a j(r)\, r\, dr$ agreed with the total current. Unless one allowed for rather exotic curves, the procedure left little room for arbitrariness and yielded fairly definite j-distributions which tended to be in reasonable accordance with experimental conductivity profiles. Thus the appearance of sawteeth greatly alleviated the need for direct measurements. In addition to that, Kadomtsev's theory provided a rather stringent criterion by which the reliability of a new experimental technique could be judged. A good example to illustrate this point is the Thomson scattering measurement performed on the DITE Tokamak in 1978 (cf. Section 5.2). Although the authors found a central safety factor of about 0.84 and claimed an accuracy of 5%, this observation was hardly noticed and did not in any

way shake the prevailing conception. It is, therefore, not surprising that the vast majority of publications dealing with measurements of magnetic fields or current densities concentrates on the plasma core region and lays emphasis on the magnitude of $q(0)$.

Unfortunately, a compilation of the relevant data produces a rather confusing picture which is well exemplified by the inconsistent results obtained on the TEXT device. Depending on the measurement technique, the central safety factor in similar discharges was determined to be less than 0.5 (from pellet injection studies, Section 6.1), approximately equal to 0.8 (by lithium beam spectroscopy, Section 4.1), and very close to unity (by polarization spectroscopy of intrinsic impurities, Section 3.4, and of injected lithium atoms, Section 4.1). The extremely low value of the pellet technique has been called into question because of interpretative difficulties, but the papers reporting the latter two results give the impression that they provide equally conclusive, though contradictory, information on the sawtooth collapse (i.e. either against or in favour of the Kadomtsev model). Other experiments, which support the conventional view of $q(0)$ being close to one, were performed on the ATC machine (fast ion orbits, Section 4.3), on ASDEX (lithium beam spectroscopy, Section 4.1), and on TCA (resonant Alfvén waves, Section 6.2). In contrast to these observations, low values of $q(0) \lesssim 0.8$ were found in PBX-M and DIII-D (motional Stark effect, Section 4.2), in TEXTOR and JET (Faraday rotation technique, Section 5.3), in PDX (fast ion orbits, Section 4.3) and again in TEXTOR (discrete Alfvén waves, Section 6.2). Direct magnetic probe measurements in the small TOKAPOLE II device yielded $q(0) \simeq 0.7$ without detectable changes during a sawtooth period (MOYER *et al.*, 1989).

In an attempt to reconcile the seemingly incompatible results, WESTERHOF (1987) proposed the assumption of at least two different mechanisms for the sawtooth activity. However, while it is quite plausible to anticipate a strong impact of operational measures like additional heating and current drive, conspicuous discrepancies exist already for Ohmic discharges with very regular and reproducible sawtooth oscillations. For these latter conditions more detailed experiments were carried out on TEXTOR (SOLTWISCH, 1988) and JET (O'ROURKE, 1991) in order to resolve the temporal behaviour of $q(0)$ throughout a sawtooth cycle. In both investigations the central safety factor turned out to be slightly modulated with a variation of $\lesssim 8\%$ of the average value. Although the observed sawtoothlike waveform of $q_0(t)$ indicated a rapid magnetic field redistribution in conjunction with the collapse, a complete reconnection of the poloidal flux did not occur because the axial safety factor stayed well below one. For the JET experiment this conclusion was corroborated by field diffusion calculations which were not able to reproduce the measurements under the assumption of periodic complete reconnections.

Besides the intensive studies of $q(0)$ in relation to the sawtooth phenomenon, few other topics have been addressed. Firstly, some of those techniques that allowed the determination of complete profiles of the safety factor or current density were employed to check the theories of classical and neo-classical resistivity (cf. Section 3.1). WRÓBLEWSKI *et al.* (1988a) found significantly broader j-profiles than predicted by either of the models and inferred from this a decoupling of the current and temperature distributions. They performed their measurements in Ohmically heated (OH) discharges of relatively low densities in the TEXT Tokamak by means of polarization spectroscopy of an impurity ion line (Section 3.4). MCCORMICK *et al.* (1987)

used the technique of lithium beam spectroscopy (Section 4.1) in low-density OH discharges in ASDEX and derived current densities which were in-between the classical and neo-classical values (with a tendency towards the former). However, the authors pointed out that the available data were not well suited to a decision as to which resistivity model was more correct. Faraday rotation measurements on TEXTOR (SOLTWISCH *et al.*, 1984) provided considerable evidence in favour of the neo-classical theory for OH plasmas at intermediate densities, but also here the overall uncertainties in j, T_e and Z_{eff} prevented an unambiguous answer to the question of trapped electrons.

Secondly, the effects of lower-hybrid current drive (LHCD) on the j-profile in ASDEX were investigated by MCCORMICK *et al.* (1987). The main result was a substantial broadening of the current density distribution which raised the central safety factor well above one and so explained the observed disappearance of sawteeth. Figure 12 shows the j- and q-profiles before (OH) and during LHCD as measured by lithium beam spectroscopy in a discharge with $\bar{n}_e = 7 \times 10^{18}$ m^{-3} and $q(a) = 3.4$.

Finally, an attempt was made to take up the subject of "profile consistency" and to represent a variety of measured j-distributions by a universal profile in properly reduced co-ordinates (SOLTWISCH *et al.*, 1986b). The data base comprised OH discharges in TEXTOR with the safety factor at the limiter ranging from 2.1 to 6.3. In quasi-stationary conditions with regular sawtooth activity the profiles assumed a unique shape by displaying j in units of $B_t/(\mu_0 R)$ and r in units of $(\mu_0 RI/B_t)^{1/2}$ (here, B_t is the toroidal field, I is the total plasma current, and R denotes the major plasma radius; see Fig. 10 in Section 5.3). The existence of the universal profile was attributed to the combined effects of a thermal instability (causing a shrinkage of the current channel) and a periodically enhanced transport in the core region due to sawteeth (halting the contraction and providing a link with the adjustable parameters B_t, I and R through the location of the $q = 1$ surface). An extension of these studies to discharges with strong additional heating has as yet not been made.

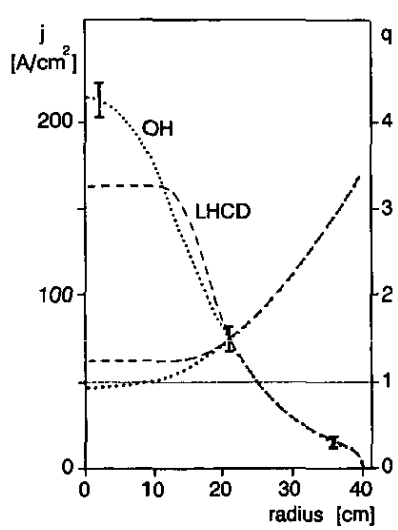

FIG. 12.—Current densities and cylindrical q-profiles before (OH) and during (LHCD) lower-hybrid current drive in a ASDEX discharge with $\bar{n}_e = 7 \times 10^{18}$ m^{-3} and $q(a) = 3.4$ (after MCCORMICK *et al.*, 1987).

The important issue of current penetration during the start-up phase of Tokamak discharges is still awaiting detailed time-resolved measurements of the current density distribution. The present understanding relies, in the main, on rather indirect information gleaned from equilibrium code calculations together with such evidence as could be obtained from kinetic measurements and observations of MHD activity. MEYERHOFER *et al.* (1985) endeavoured to supplement these data by the temporal evolution of the central safety factor which they determined for a few selected PDX discharges by means of the Fast-Ion Diagnostic Experiment (cf. Section 4.3). BRÜSSAU (1989) used the Faraday rotation diagnostic on TEXTOR to investigate the relaxation of the skin current profile for a variety of discharge parameters. However, these studies are far from being comprehensive, and the subject calls for a systematic application of advanced techniques, particularly in view of the planning of a high-current device.

In summary, the present state of the art of current density measurements in Tokamak plasmas is rather unsatisfactory with respect to the technical maturity of most approaches as well as the diversity of the obtained results. On the other hand, there is a growing demand for an experimental verification of refined theoretical models and for a reliable assessment of increasingly complex discharge scenarios which cannot be done without a precise knowledge of the confining magnetic field structure. Considering the efforts spent in the past years, it seems illusory to expect a major progress towards a routine diagnostic from future large devices which are bound to leave little or no room for improvization and gradual improvements of complicated instrumentations. Therefore, a number of adaptable medium-sized Tokamak installations will be indispensable to the necessary exploration of novel concepts, the systematic development of proven schemes and a detailed investigation of basic processes related to the magnetic confinement of high-temperature plasmas.

REFERENCES

ALLADIO F. and MARTONE M. (1977) *Phys. Lett.* **60A**, 39.
BARTH C. J. (1989) *Rev. Scient. Instrum.* **60**, 2673.
BARTLETT D. V., BICKERTON R. J., BRUSATI M. *et al.* (1988) *Nucl. Fusion* **28**, 73.
BEHN R., DE CHAMBRIER A., COLLINS G. A. *et al.* (1984) *Plasma Phys. Contr. Fusion* **26**, 173.
BOILEAU A., VON HELLERMANN M., MANDL W. *et al.* (1989) *J. Phys. B: At. Mol. Opt. Phys.* **22**, L145.
BRAITHWAITE G., GOTTARDI N., MAGYAR G. *et al.* (1989) *Rev. Scient. Instrum.* **60**, 2825.
BRIZARD A., GREK B., LEBLANC B. and JOHNSON D. (1986) *Rev. Scient. Instrum.* **57**, 1813.
BRÜSSAU W. D. (1989) KFA Report Jül-2258, Forschungszentrum Jülich.
CANO R., FIDONE I. and HOSEA J. C. (1975) *Physics Fluids* **18**, 1183.
CAROLAN P. G. (1977) *Plasma Phys.* **19**, 757.
CAROLAN P. G., FORREST M. J., GOWERS C. W. and NIELSEN P. (1990) *Rev. Scient. Instrum.* **61**, 2926.
DELLIS A. N. and HOSEA J. C. (1973) Princeton Plasma Physics Laboratory Report MATT 969, Princeton University.
DEMARCO F. and SEGRE S. E. (1972). *Plasma Phys.* **14**, 245.
DESCAMPS P., VAN WASSENHOVE G., KOCH R. *et al.* (1990) *Phys. Lett.* **143A**, 311.
DURST R. D., PHILLIPS P. E. and ROWAN W. L. (1988) *Rev. Scient. Instrum.* **59**, 1623.
EDWARDS A. W., CAMPBELL D. J., ENGELHARDT W. W. *et al.* (1986) *Phys. Rev. Lett.* **57**, 210.
FELDMAN U., SEELY J. F., SHEELEY N. R., SUCKEWER S. and TITLE A. M. (1984) *J. Appl. Phys.* **56**, 2512.
FIDONE I., GRANATA G. and TEICHMANN J. (1971) *Physics Fluids* **14**, 737.
FORREST M. J., CAROLAN P. G. and PEACOCK N. J. (1978) *Nature* **271**, 718.
FUKAO M., MORI K. and TANIHARA T. (1991) *Plasma Phys. Contr. Fusion* **33**, 199.
GILL R. D., EDWARDS A. W. and WELLER A. (1989) *Nucl. Fusion* **29**, 821.
VON GOELER S., STODIEK W. and SAUTHOFF N. (1974) *Phys. Rev. Lett.* **33**, 1201.
GOLDSTON R. J. (1978) *Physics Fluids* **21**, 2346.

GOLDSTON R. J. (1982) in *Diagnostics for Fusion Reactor Conditions*, Varenna 1982 (Edited by P. E. STOTT *et al.*), Vol. 1, p. 263. CEC, Brussels.
GRAD H. and RUBIN H. (1958) *Proc. 2nd UN International Conf. Peaceful Use of Atomic Energy*, Geneva 1958, Vol. 31, p. 190. Columbia University Press, New York.
GRANETZ R. S. and CAMACHO J. F. (1985) *Nucl. Fusion* **25**, 727.
GRANETZ R. S. and SMEULDERS P. (1988) *Nucl. Fusion* **28**, 457.
HIRSHMAN S. P., HAWRYLUK R. J. and BIRGE B. (1977) *Nucl. Fusion* **17**, 611.
HUANG L. K., FINKENTHAL M., WRÓBLEWSKI D. *et al.* (1990) *Physics Fluids* **B2**, 809.
JACOBSON A. R. (1977) Los Alamos Nat. Lab. Rep. No. LA-6875-MS, Los Alamos.
JANICKI C., DECOSTE R. and SIMM C. (1989) *Phys. Rev. Lett.* **62**, 3038.
JOBES F. C. (1975) in *Plasma Diagnostics and Data Acquisiton Systems*, Varenna 1975 (Edited by A. EUBANK and E. SINDONI), p. 158. Editrice Compositori, Bologna.
JOBES F. C. and HICKOK R. L. (1970) *Nucl. Fusion* **10**, 195.
KADOMTSEV B. B. (1975) *Fiz. Plasmy* **1**, 750 [*Sov. J. Plasma Phys.* **1**, 389].
KUGEL H. W., GAMMEL G. M., KAITA R., REUSCH M. F. and ROBERTS D. W. (1988) *Rev. Scient. Instrum.* **59**, 1635.
LAO L. L., FERRON J. R., GROEBNER R. J. *et al.* (1990) *Nucl. Fusion* **30**, 1035.
LAO L. L., ST. JOHN H., STAMBAUGH R. D., KELLMAN A. G. and PFEIFFER W. (1985) *Nucl. Fusion* **25**, 1611.
LEVINTON F. M., FONCK R. J., GAMMEL G. M. *et al.* (1989) *Phys. Rev. Lett.* **63**, 2060.
LÜST R. and SCHLÜTER A. (1957) *Z. Naturforsch.* **12A**, 850.
MCCORMICK K. (1986) in *Basic and Advanced Diagnostic Techniques for Fusion Plasmas*, Varenna 1986 (Edited by P. E. STOTT *et al.*), Vol. 2, p. 635. CEC, Brussels.
MCCORMICK K., KICK M. and OLIVAIN J. (1977) *Proc. 8th European Conf. on Controlled Fusion and Plasma Physics*, Prague 1977, p. 140. EPS, Geneva.
MCCORMICK K., SÖLDNER F. X., ECKHARTT D. *et al.* (1987) *Phys. Rev. Lett.* **58**, 491.
MEYERHOFER, D. D., GOLDSTON R. J., KAITA R. *et al.* (1985) *Nucl. Fusion* **25**, 321.
MOYER R. A., GOETZ J. A., DEXTER R. N. and PRAGER S. C. (1989) *Physics Fluids B* **1**, 2139.
O'ROURKE J. (1991) *Plasma Phys. Contr. Fusion* **33**, 289.
PEACOCK N. J. (1978) in *Diagnostics for Fusion Experiments*, Varenna 1978 (Edited by E. SINDONI and C. WHARTON), p. 367. Pergamon Press, Oxford.
PÉGOURIÉ B. and DUBOIS M. A. (1990) *Nucl. Fusion* **30**, 1575.
SAUTHOFF N. R., VON GOELER S. and STODIEK W. (1978) *Nucl. Fusion* **18**, 1445.
SHAFRANOV V. D. (1958) *Sov. Phys. J.E.T.P.* **6**, 545.
SHEFFIELD J. (1972) *Plasma Phys.* **14**, 385.
SOLTWISCH H. (1983) *Proc. 11th European Conf. on Controlled Fusion and Plasma Physics*, Aachen 1983, Vol. 7D, part I, p. 123. EPS, Geneva.
SOLTWISCH H. (1986a) in *Basic and Advanced Diagnostic Techniques*, Varenna 1986 (Edited by P. E. STOTT *et al.*), Vol. 2, p. 343. CEC, Brussels.
SOLTWISCH H. (1988) *Rev. Scient. Instrum.* **59**, 1599.
SOLTWISCH H., GRAFFMANN E., SCHLÜTER J. and WAIDMANN G. (1984) *Proc. International Conf. on Plasma Physics*, Lausanne 1984 (invited papers), Vol. I, p. 499. CEC, Brussels.
SOLTWISCH H., STODIEK W., MANICKAM J. and SCHLÜTER J. (1986b) *Proc. 11th International Conf. on Plasma Physics and Controlled Nuclear Fusion Research*, Kyoto 1986, Vol. 1, p. 263. IAEA, Vienna.
SPITZER L. and HÄRM R. (1953) *Phys. Rev.* **89**, 977.
TERRY J. L., MARMAR E. S., HOWELL R.B. *et al.* (1990) *Rev. Scient. Instrum.* **61**, 2908.
TFR GROUP (1975) *Proc. 7th European Conf. on Controlled Fusion and Plasma Physics*, Lausanne 1975, Vol. I, p. 11. EPS, Geneva.
TFR GROUP (1986) *Europhys. Lett.* **2**, 267.
TFR GROUP (1987) *Nucl. Fusion* **27**, 1975.
VÉRON D. (1979) in *Infrared and Millimeter Waves* (Edited by K. J. BUTTON), Vol. 2. Academic Press, New York.
WEISEN H., BORG G., JOYE B., KNIGHT A. J. and LISTER J. B. (1989) *Phys. Rev. Lett.* **62**, 434.
WESSON J. A. (1987) *Tokamaks*. Clarendon Press, Oxford.
WEST W. P. (1986) *Rev. Scient. Instrum.* **57**, 2006.
WEST W. P., THOMAS D. M., DEGRASSIE J. S. and ZHENG S. B. (1987) *Phys. Rev. Lett.* **58**, 2758.
WESTERHOF E. (1987) *Comments Plasma Phys. Contr. Fusion* **11**, 79.
WRÓBLEWSKI D., HUANG L. K. and MOOS H. W. (1988a) *Rev. Scient. Instrum.* **59**, 2341.
WRÓBLEWSKI D., HUANG L. K., MOOS H. W. and PHILLIPS P. E. (1988b) *Phys. Rev. Lett.* **61**, 1724.
WRÓBLEWSKI D. and LAO L. L. (1991) *Physics Fluids B* **3**, 2877.
ZARNSTORFF M. C., MCGUIRE K., BELL M. G. *et al.* (1990) *Physics Fluids B* **2**, 1852.